Drag Modulation Flight Control System Options for Planetary Aerocapture

Zachary R. Putnam,* and Robert D. Braun†

Georgia Institute of Technology, Atlanta, Georgia, 30332

Drag modulation flight control may provide a simple method for controlling energy during aerocapture. Several drag modulation fight control system options are discussed and evaluated, including single-stage jettison, two-stage jettison, and continuously-variable drag modulation systems. Performance is assessed using numeric simulation with real-time guidance and targeting algorithms. Monte Carlo simulation is used to evaluate system robustness to expected day-of-flight uncertainties. Results indicate that drag modulation flight control is an attractive option for aerocapture systems at Mars where low peak heat rates enable the use of lightweight inflatable drag areas. Aerocapture using drag modulation at Titan is found to require large drag areas to limit peak heat rates to non-ablative thermal protection system limits or advanced lightweight ablators. The large gravity well and high peak heat rates experienced during aerocapture at Venus make drag modulation flight control unattractive when combined with a non-ablative thermal protection system. Significantly larger drag areas or advances in fabric-based material thermal properties are required to improve feasibility at Venus.

Nomenclature

a_A	Axial acceleration magnitude, m/s^2	S_{ref}	Aerodynamic reference area, m^2
C_A	Axial force coefficient	V	Velocity magnitude, m/s
C_D	Drag coefficient	β	Ballistic coefficient, kg/m^2
C_N	Normal force coefficient	ΔV	Change in velocity, m/s
F	Correction factor	ρ	Atmospheric density, kg/m^3
K	Filter gain	σ	Standard deviation
m	Mass, kg		

Subscript

AI	Atmospheric interface	i	Index
est	Estimate	$wind$	Wind-relative

I. Introduction

FUTURE aeroassist systems must be able to provide accurate delivery of more massive payloads than current systems to support the next generation of exploration missions. This increase in delivered payload mass may be achieved by reducing or eliminating the diameter and shape constraints placed on the aeroassist system by the launch vehicle, allowing the aeroassist vehicle to assume an aerodynamic form that best facilitates mission success. Deployable aerodynamic devices, both rigid and inflatable, have the potential to enable a broad spectrum of next-generation missions by mitigating launch vehicle payload fairing shape and size constraints on aeroassist vehicles and potentially providing an in-flight reconfiguration capability. Deployable aerodynamic devices also enable new options for trajectory control during atmospheric flight.

---

*Graduate Research Assistant, School of Aerospace Engineering, 270 Ferst Drive, Senior Member AIAA.

†Professor, School of Aerospace Engineering, 270 Ferst Drive, AIAA Fellow.

One new option is drag modulation flight control. Increasing the vehicle drag area decreases β (see Eq. (1)) and the energy depletion rate. Increasing β has the opposite effect. Therefore, an aeroassist vehicle that can vary β is capable of controlling its energy or downrange. For a vehicle of mass m, drag modulation utilizes changes in drag area, $C_D S_{ref}$, to change β during atmospheric flight to control the vehicle trajectory, either through changes in S_{ref} or C_D.
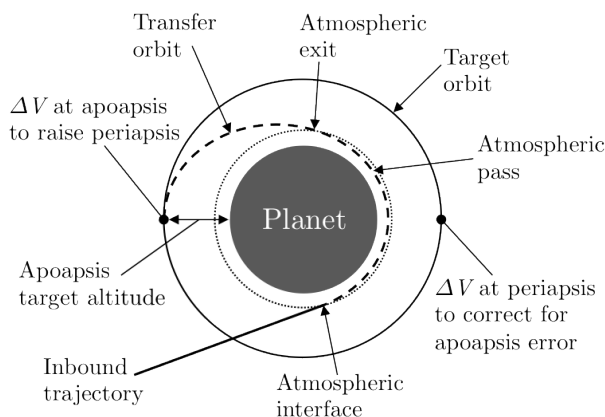
$$\beta = \frac{m}{C_D S_{ref}} \tag{1}$$

Hypersonic inflatable aerodynamic devices (HIADs), a technology currently being developed by NASA for use in aeroassist applications, have been featured prominently in recent NASA studies for human Mars exploration.[1,2] While the HIAD development program will lead to mature inflatable devices suitable for drag modulation flight control applications, most studies to date have not considered drag modulation as a flight control option. Instead, they have assumed that lift modulation flight control is possible for these types of vehicles, either though bank angle or angle-of-attack modulation. However, effector requirements for large inflatable vehicles may make lift modulation infeasible or undesirable. For these types of vehicles, drag modulation presents a solution that does not require complex effectors or asymmetric flight conditions. Drag modulation is particularly attractive for aerocapture trajectories, as the absence of out-of-plane control authority may be less critical than for entry, descent, and landing systems where landing precision is increasingly important.[3] Additionally, post-atmospheric pass propulsive maneuvers are baselined for nominal aerocapture sequences and may be used to correct out-of-plane errors.

Only a small number of studies on using drag modulation for aeroassist missions are available in the literature. In the 1960s, Levy determined a closed-form solution using drag modulation to limit the rate of increase of deceleration during entry[4] and Rose and Hayes evaluated drag modulation as means for orbit phasing and entry targeting.[5] More recently, Kuo et al. examined the use of drag modulation to track reference trajectories for ballistic missiles.[6] These studies all assumed drag could be controlled continuously within a given interval. Discrete-event drag modulation has been studied for planetary aerocapture missions at the conceptual level, but few studies address realistic guided system performance.[7–9] Miller et al. present a real-time predictive algorithm for single-stage jettison aerocapture at Titan using a trailing toroidal ballute.[10] Johnson and Lyons use a heuristic trigger based on curve fits of the aerocapture vehicle dynamics to perform single-stage jettison aerocapture at Titan.[11]

This study considers the use of drag modulation flight control systems for planetary aerocapture systems. The aerocapture maneuver is utilized to transition from a high-energy orbit to a lower-energy orbit without a major propulsive event, as shown in Fig. 1. Aerocapture differs from aerobraking in that it depletes the required energy in a single atmospheric pass instead of a series of passes. Aerocapture systems still require propulsive capability: after the atmospheric pass, the spacecraft must perform a periapsis raise maneuver at apoapsis to ensure that the vehicle does not reenter the atmosphere. An additional propulsive cleanup maneuver may also be performed at the subsequent periapsis to correct any remaining error in apoapsis altitude.

Recent work has shown that drag modulation may be possible for a specific set of aerocapture missions at Earth and Mars.[12] The goal of this study

Figure 1. Example aerocapture maneuver.

is to expand upon those results by determining the feasibility and relative performance of different drag modulation flight control system options for planetary aerocapture at Venus, Mars, and Titan. Three drag modulation flight control system options will be considered: single-stage jettison, two-stage jettison, and continuously-variable drag modulation systems.

American Institute of Aeronautics and Astronautics

II.   Drag Modulation Flight Control Concepts

A.   Single-stage Jettison Systems

Single-stage jettison systems, shown in Fig. 2, provide the simplest means of drag modulation flight control for aerocapture. The vehicle deploys a large drag skirt prior to atmospheric interface (AI) to lower the vehicle's β to its minimum value, β_1. Alternately, the vehicle may launch in its β_1 configuration if the maximum diameter fits within the launch vehicle payload fairing. During the atmospheric pass, the flight computer uses available navigation data to determine when the drag skirt should be jettisoned such that the proper amount of energy is dissipated prior to atmospheric exit to achieve the desired transfer orbit properties. Once the drag skirt is jettisoned, β immediately rises to its maximum value, β_2, and the spacecraft coasts to atmospheric exit.

While simple, single-stage jettison systems are vulnerable to day-of-flight dispersions since they have only a single control event. After the jettison, no control authority is available to correct for unforeseen dispersions. Mission designers may bias the nominal jettison point towards the end of the atmospheric pass to reduce the effect of post-jettison uncertainty, but this strategy requires additional control authority and increases the likelihood of a skip-out trajectory.
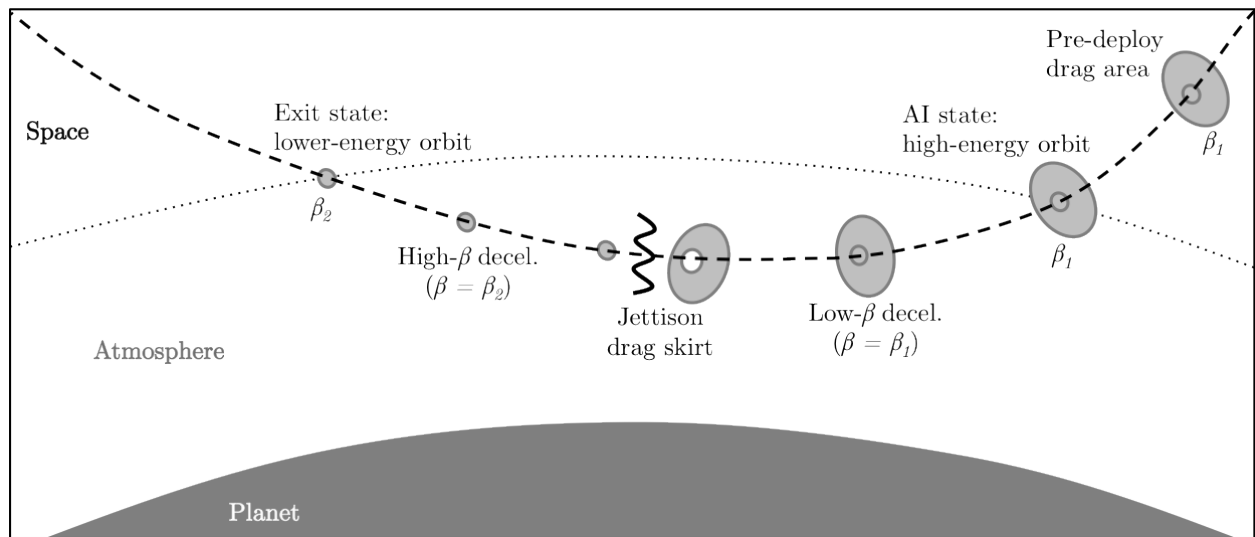

Figure 2.   Single-stage jettison drag modulation aerocapture system.

B.   Two-stage Jettison Systems

In some circumstances, two-stage jettison systems provide performance benefits over a single-stage systems by reducing vulnerability to day-of-flight dispersions. A two-stage system splits the drag skirt into two concentric pieces, allowing the spacecraft to perform a "clean-up" jettison later in the trajectory. This drag modulation strategy trades additional system complexity for reduced susceptibility to unforeseen late-trajectory dispersions.

Figure 3 shows a notional aerocapture maneuver using a two-stage jettison drag modulation system. As in the single-stage system, the drag skirts are deployed prior to AI and the vehicle enters the atmosphere with $\beta = \beta_1$. The outer drag skirt is jettisoned first, such that the final apoapsis error is minimized while assuming a pre-set inner skirt jettison time. The outer skirt jettison changes β to an intermediate value, β_3. The inner drag skirt jettison time is then adjusted to null the final transfer orbit apoapsis altitude error. When the inner drag skirt is jettisoned, β rises to β_2 and the spacecraft coasts to atmospheric exit. This strategy allows the flight computer to solve two one-dimensional searches in series, reducing flight software complexity and limiting computational resource requirements.
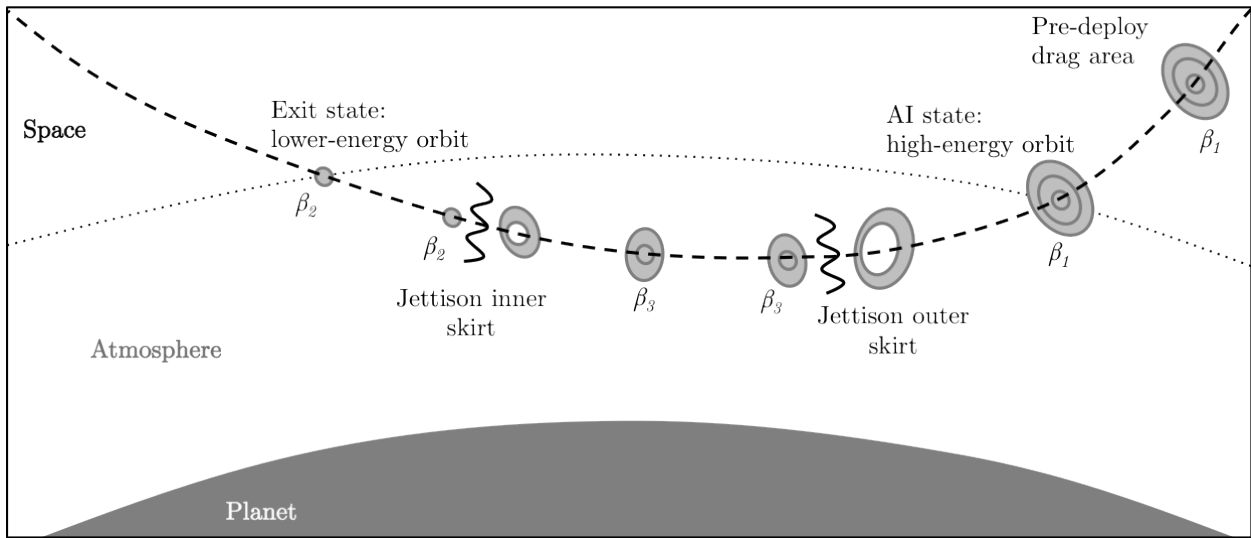
American Institute of Aeronautics and Astronautics

Figure 3. Two-stage jettison drag modulation aerocapture system.

C. Continuously-variable Systems

As the number of jettison stages becomes large, a staged-jettison vehicle may be approximated by a one-directional continuously-variable drag modulation system. However, it is likely that such a system would be capable of both decreasing and increasing β. This continuously-variable (CV) drag modulation system uses a drag skirt that can be deployed and retracted during the atmospheric pass. While this in-flight reconfiguration capability requires significant technology development, current technology programs indicate that such a system may be feasible.[13]

The CV drag modulation system concept analyzed in this study is shown in Fig. 4. The vehicle enters the atmosphere with its drag skirt deployed. During the atmospheric pass, the vehicle determines the constant drag area that minimizes the final apoapsis altitude error, subject to limits β_1 and β_2. This type of system retains a measure of control authority throughout the atmospheric pass, but requires a more mechanically complex system relative to staged-jettison systems.
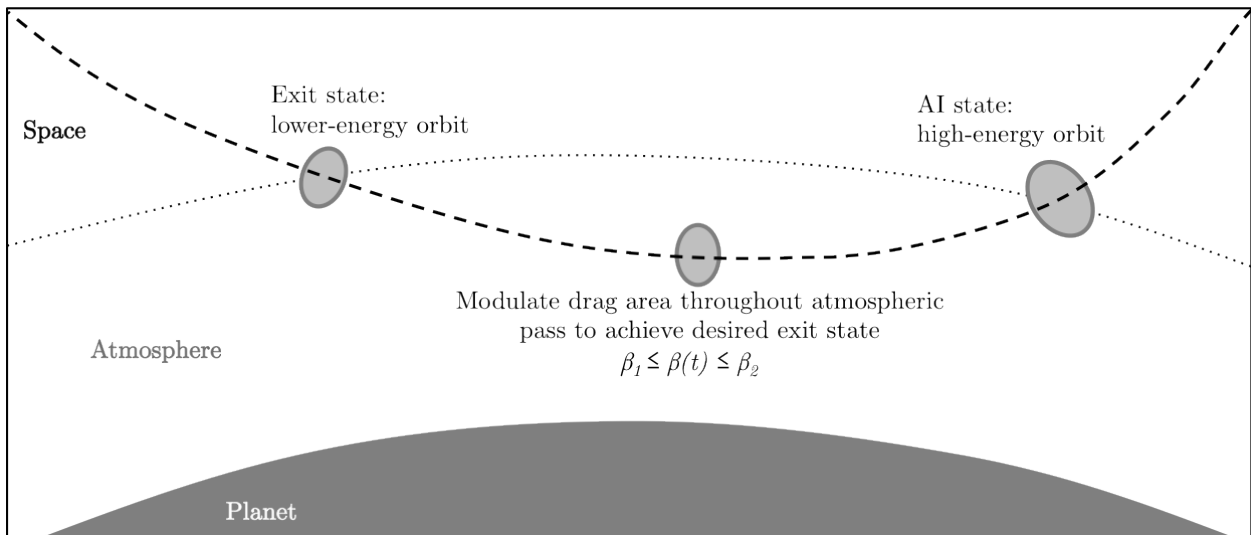

Figure 4. Continuously-variable drag modulation aerocapture system.

D.   Real-time Guidance

During the atmospheric pass, a real-time guidance algorithm is used to determine drag skirt jettison times and drag area commands using data from the navigation system. This strategy allows the vehicle to select a drag profile based on day-of-flight conditions such that the desired transfer orbit is achieved. A similar algorithm is used for all three drag modulation system options.

The guidance algorithm is organized into three functional phases. The first phase is the pre-AI attitude hold phase. During this phase, the guidance algorithm checks whether the sensible atmosphere has been reached. The sensible atmosphere is defined by sensed accelerations greater than 0.5 m/s^2. The second phase is the numeric predictor-corrector (NPC) targeting phase. During this phase, the algorithm adjusts the jettison time or drag area command to minimize the final apoapsis altitude error. The third and final phase is the exit phase: no additional commands are issued when the sensed acceleration drops below 0.5 m/s^2.

1.   Numeric Predictor-corrector

The predictor integrates the three-degree-of-freedom equations of motion using a 4th-order Runge-Kutta method to determine the vehicle state at atmospheric exit. The predictor models the planetary body of interest as a sphere with inverse-square gravity and a nominal altitude-density atmosphere table. The vehicle is modeled as a point mass that generates only drag; vehicle drag is modeled with a constant C_D. While the majority of the integration is performed with a constant time step of 2 s, the time steps immediately adjacent to jettison events are adjusted such that the jettisons occur at a major time step. This strategy enhances the accuracy and stability of the prediction without significantly increasing the computation time. Nominally, prediction terminates at atmospheric exit, defined by a maximum altitude. Protection is provided within the predictor against off-nominal cases through limits on integration time and minimum altitude.

The corrector utilizes the terminal states computed by the predictor to determine jettison times for the staged-jettison systems or drag area commands for CV systems. First, the corrector computes the properties of the transfer orbit from the estimated terminal vehicle position and velocity vectors at atmospheric exit. Next, the corrector attempts to bound the solution. If the transfer orbit semi-major axis is negative, indicating a hyperbolic escape trajectory, the corrector marches the command towards the capture region, either by increasing the jettison time or increasing the drag area. The predictor is then re-run until the corrector has found a non-hyperbolic, captured solution for the jettison time (staged systems) or drag area (CV systems). If the first captured solution has a positive apoapsis error, indicating overshoot, the corrector marches towards towards the crash region until an undershoot solution is found. The opposite is done if the first capture solution has a negative apoapsis error. Once the solution is bounded, bisection is used to determine a solution that nulls the transfer orbit apoapsis error. Bisection continues until either the iteration limit is reached or the change in command is less than a pre-set threshold. If no solution is found, the previous best estimate of jettison time or drag area is used.

2.   Atmospheric Density Estimation

The guidance algorithm estimates a constant bias atmospheric density correction factor to account for day-of-flight uncertainty in the atmosphere and improve the accuracy of terminal state predictions. The current density is estimated from navigated acceleration and velocity and the onboard atmosphere model, as shown in Eq. 2. Neither a_A or V_{wind} are available directly in the absence of a flush air data system, so they are approximated with the sensed acceleration magnitude and the planet-relative velocity magnitude. The density correction factor, F_{est}, is then computed as shown in Eq. (3). Using a factor allows the predictor to update the onboard atmosphere model data by a multiplying the density data by a constant parameter. To improve the estimate, the factor is limited to minimum and maximum values and filtered with the previous value, F_{i-1}, using the low-pass filter in Eq. (4). A gain, K, of 0.05 provides a good balance between reducing noise and capturing short-period changes in the atmosphere relative to the onboard atmosphere model. The bounded, filtered estimate is then stored for use in the predictor.

$$\rho_{est} = \frac{2ma_A}{V_{wind}^2 S_{ref} C_A} \tag{2}$$

$$F_{est} = \frac{\rho_{est}}{\rho_{model}} \tag{3}$$

$$F_i = (1 - K) F_{i-1} + K F_{est} \tag{4}$$

III. Methodology

A. Numeric Simulation

A three-degree-of-freedom simulation was used in this study to evaluate drag modulation system aerocapture flight performance. The simulation is written in Matlab and autocoded to C and compiled to improve execution speed. The equations of motion are integrated using a 4th order Runge-Kutta integration scheme with a constant time step. Planetary bodies are modeled as spheres with inverse square gravity. Planetary atmospheres are modeled using a table look-up of atmospheric properties stored as a function of altitude. Planetary atmosphere data for Mars, Venus, and Titan were generated using the Global Reference Atmosphere Models (GRAM) for each planetary body.[14] Stagnation-point convective heat rates are estimated using the Sutton-Graves relation for a 1 m reference nose radius.[15] Radiative contributions to total heat rate are significant at Venus and Titan, but are not modeled. A summary of planetary model parameters is given in Table 1. Two-body orbital mechanics are used to compute the ΔV required for periapsis raise and apoapsis correction maneuvers.

Table 1. Planetary Model Parameters

Parameter	Mars	Titan	Venus
Gravitational parameter, m^3/s^2	4.283 $\times 10^{13}$	8.9797 $\times 10^{12}$	3.249 $\times 10^{14}$
Volumetric mean radius , m	3.3895 $\times 10^6$	2.575 $\times 10^6$	6.0518 $\times 10^6$
Atmospheric interface altitude, km	150 km	1700 km	150 km
Atmosphere model	Mars-GRAM	Titan-GRAM	Venus-GRAM
Sutton-Graves coefficient, kg$^{0.5}$/m	1.898$\times 10^{-4}$	1.7407 $\times 10^{-4}$	1.986 $\times 10^{-4}$

Aerocapture vehicles were assumed to have constant mass. A 70-deg spherecone shape was assumed for Mars and Titan missions and a 60-deg spherecone shape was assumed for Venus missions. Mach-dependent aerodynamics data were generated for these shapes using CBAero.[16] For all three drag modulation system options, drag modulation is accomplished through changes in S_{ref}; aerodynamic coefficients were assumed to be constant across all S_{ref} changes. The nominal vehicle center of gravity (c.g.) position is along the vehicle axis of symmetry. The vehicles are spun about their axis of symmetry at 2 RPM to reduce the effect of lift generated by off-nominal c.g. positions. The flight computer was modeled with two rate groups: a low rate group for guidance running at 0.25 for Titan and 0.5 Hz for Venus and Mars and a high rate group for control, running at 25 for Titan and 50 Hz for Venus and Mars. These rates reflect differences in flight times at Venus, Mars, and Titan. The onboard inertial navigation system was assumed to have perfect knowledge of the vehicle dynamics.

B. Monte Carlo Simulation

Monte Carlo simulation was used to evaluate aerocapture system performance at Mars and Titan in the the presence of day-of-flight uncertainties, including state, vehicle, and environmental uncertainties. Monte Carlo simulation uncertainty inputs are given in Table 2. Correlated state errors for Mars are generated based on 3σ 1.5 km position and 1 m/s velocity errors, corresponding to Mars Science Laboratory (MSL) approach navigation performance.[17] State errors for Titan are uncorrelated. At Titan, current navigation technology can provide a 3σ flight-path angle variation of 0.24 deg for aerocapture missions.[18] Other state errors were computed based on the results presented in Ref. 19 and were scaled such that the flight-path angle uncertainty matched current capabilities. Correlated atmospheric density and wind uncertainties were generated using Mars-GRAM and Titan-GRAM.

American Institute of Aeronautics and Astronautics

Table 2. Monte Carlo Simulation Input

Parameter	Dispersion min/max or 3σ	Notes
	Mars	
Atmospheric density and wind	Mars-GRAM	Default settings for 5 August 2012
Hypersonic C_A	3%	70 deg sphere-cone[20]
Hypersonic C_N	5%	70 deg sphere-cone[20]
Trim angle of attack	2 deg	Accounts for off-centerline c.g.
Initial bank angle	± 180 deg	Covers all possible c.g. offset orientations
Bank angle rate	5%	
Vehicle mass	3 kg	
AI velocity	0.49 m/s	Correlated MSL error[17]
AI flight-path	0.013 deg	Correlated MSL error[17]
AI azimuth	0.0075 deg	Correlated MSL error[17]
AI latitude	0.017 deg	Correlated MSL error[17]
AI longitude	0.012 deg	Correlated MSL error[17]
AI altitude	0.74 km	Correlated MSL error[17]
	Titan	
Atmospheric density and wind	Titan-GRAM	Default settings
Hypersonic C_A	3%	70 deg sphere-cone[21]
Hypersonic C_N	5%	70 deg sphere-cone[21]
Trim angle of attack	2 deg	Accounts for off-centerline c.g.
Initial bank angle	± 180 deg	Covers all possible c.g.-offset orientations
Bank angle rate	5%	
Vehicle mass	3 kg	
AI velocity	4.2 m/s	Uncorrelated, approximated from Ref. 19
AI flight-path	0.24 deg	Titan Explorer value[18]
AI azimuth	0.022 deg	Uncorrelated, approximated from Ref. 19
AI latitude	0.030 deg	Uncorrelated, approximated from Ref. 19
AI longitude	0.23 deg	Uncorrelated, approximated from Ref. 19
AI altitude	10.4 km	Uncorrelated, approximated from Ref. 19

IV. Corridor and Feasibility

A. Corridor Definition

For aerocapture drag modulation flight control systems, the aerodynamic corridor is bounded by the minimum-β (β_1) and maximum-β (β_2) trajectories. These bounding trajectories represent the most shallow and most steep trajectories, respectively, that may be flown while reaching a given transfer orbit, regardless of the type of drag modulation system employed. For single-stage systems, these trajectories represent either retaining the drag skirt to atmospheric exit (maximum drag area throughout the atmospheric pass) or jettisoning it at AI (minimum drag area throughout the atmospheric pass). For CV systems, these trajectories represent flight at a constant β of β_1 or β_2 throughout the atmospheric pass. The set of AI flight-path angles bounded by the AI flight-path angles of these trajectories is the aerodynamic flight-path angle corridor. For a given AI velocity, with perfect state knowledge, a drag modulation aerocapture vehicle that can vary β between β_1 and β_2 should be able to reach the desired transfer orbit as long as the AI flight-path angle lies within the corridor.

   Figure 5 shows example bounding trajectories for aerocapture at Mars at an inertial AI velocity of 6 km/s with a 400 km apoapsis altitude transfer orbit target for a vehicle with $\beta_1 = 10$ kg/m^2 and $\beta_2 = 100$ kg/m^2. AI is denoted by squares and atmospheric exit by triangles. Figure 5(a) shows that the β_2 trajectory decelerates about 20 km lower in the atmosphere. The β_2 trajectory must enter the atmosphere at a steeper flight-path angle, and exists with a slightly less shallow flight-path angle, as shown in Fig. 5(b). Figure 5(c) shows the deceleration pulses are similar for both cases. The ΔV required for the periapsis raise maneuver is similar for both cases: 97.9 and 97.7 m/s for the β_1 and β_2 trajectories, respectively.
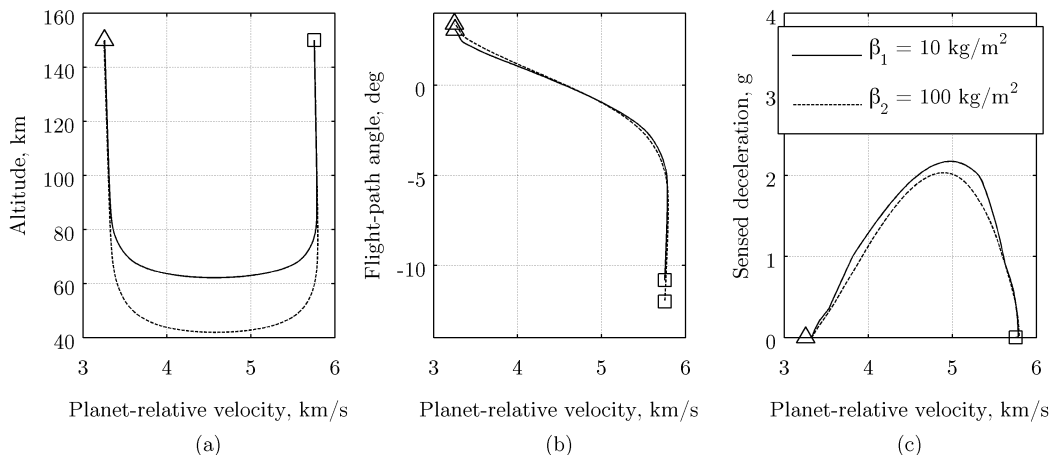

Figure 5. Example bounding trajectories for aerocapture aerodynamic corridor at Mars: (a) altitude, (b) flight-path angle, and (c) sensed deceleration versus planet-relative velocity.

B. Corridor Trends

Corridor trends were evaluated at Mars with respect to vehicle and mission design quantities; similar trends emerge for aerocapture at Titan and Venus. Figure 6 shows how the aerodynamic corridor changes with respect to AI velocity for several values of β. The corridor width for a given drag modulation system corresponds to the distance between the two curves corresponding to the β_1 and β_2 for that vehicle. Similar to atmospheric entry, the corridor steepens and widens as AI velocity increases, but at high velocities, trajectory constraints on deceleration or heat rate may reduce the width of the corridor. Figure 7 shows the aerodynamic flight-path angle corridor width as a function of β-ratio for four AI velocities, where β-ratio is the ratio of β_2 to β_1. β-ratio is a measure of the gross control authority of a drag modulation system.[12] A β-ratio of 1 results in a zero-width corridor, since $\beta_1 = \beta_2$. Increasing the β-ratio or AI velocity increases the width of the corridor with diminishing returns.

   Figure 8 shows the variation in aerodynamic corridor width with respect to β_1, for an AI velocity of 6 km/s . For all but the smallest values of β_1, corridor width is constant with respect to β_1 and determined

American Institute of Aeronautics and Astronautics

by β-ratio. This implies that only the relative change in β of a given vehicle is important for determining corridor width, not the values of β_1 or β_2.
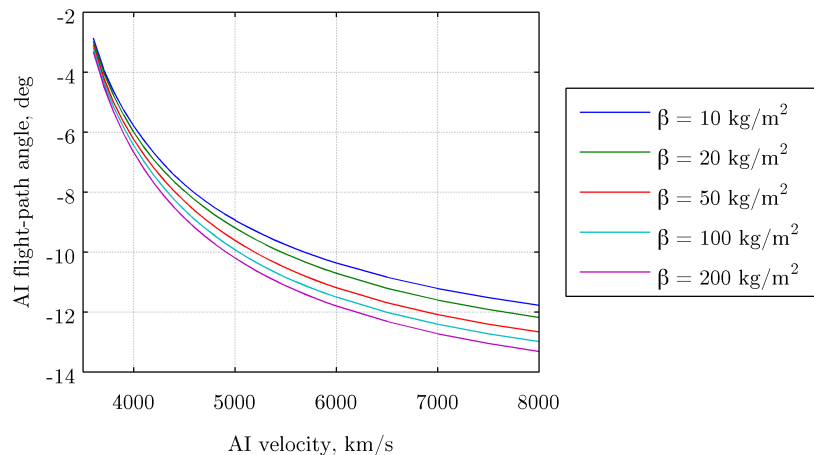

Figure 6. Aerocapture corridor bounding AI flight-path angles versus AI velocity for several β at Mars.
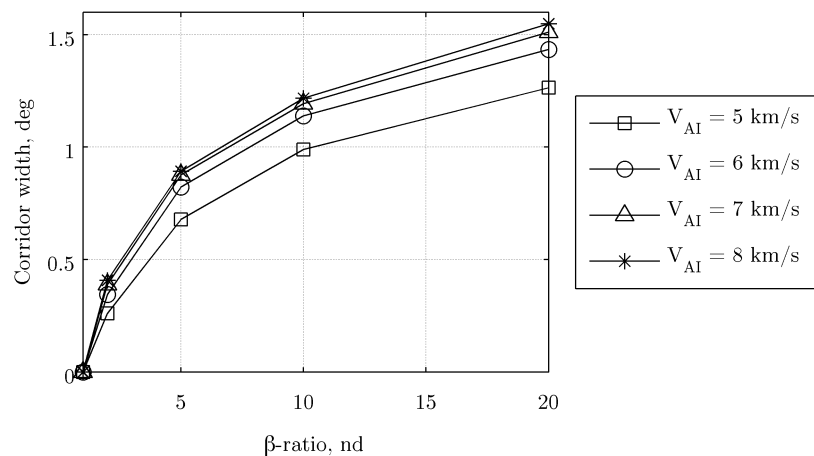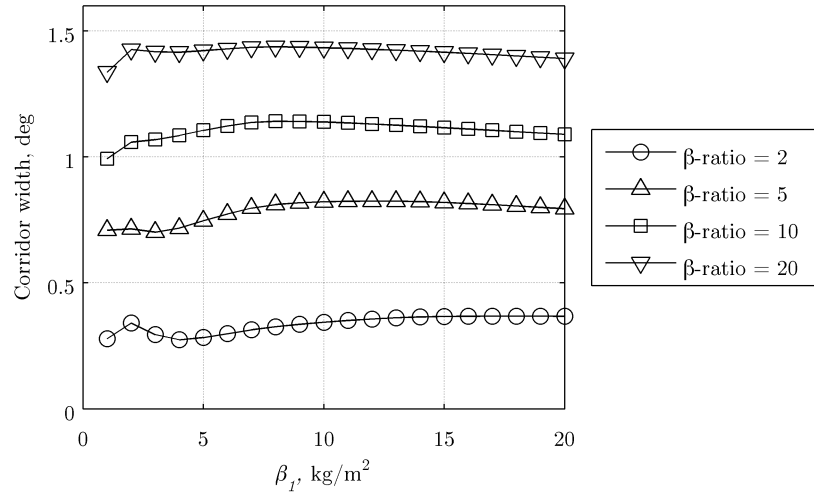

Figure 7. Aerodynamic corridor width as a function of β for several AI velocities at Mars.

C. Feasibility

Aerodynamic flight-path angle corridor width was evaluated as a function of AI velocity for aerocapture at Mars, Titan, and Venus. The AI velocity range for Mars was selected to capture a range of launch opportunities from Earth, consistent with the efficient trajectories used for robotic missions.[22] The Titan AI velocity range spans Titan escape velocity to 10 km/s, the upper bound on approach velocities assumed by Lockwood.[21] Venus AI velocities were selected to correspond to existing literature.[23] The transfer orbit apoapsis altitude target of 400 km is used at Venus and Mars and an apoapsis altitude target of 1700 km is used at Titan. The results presented in Fig. 9 show that, for a given β-ratio, corridor width at Mars is approximately double that at Venus, and corridor width at Titan is nearly two and a half times that at Mars. With identical approach navigation precision, aerocapture at Venus would require twice as much control authority as aerocapture at Mars. However, approach navigation at Venus is likely less precise, requiring even more control authority relative to Mars. This translates to a larger required initial drag area for a given spacecraft mass. At Titan, less control authority is required for a given approach navigation precision. However, approach navigation at Titan is significantly less precise than at Mars, reducing the

American Institute of Aeronautics and Astronautics

Figure 8. Aerodynamic corridor width as a function of β_1 for several β-ratios at Mars for AI velocity of 6 km/s.

impact of this advantage. As discussed in the previous section, Fig. 9 shows that β-ratio is the primary factor determining corridor width, corridor width increases a modest amount with increasing AI velocity, and β_1 has only a small effect on the corridor width.

Figure 10 shows peak stagnation-point convective heating rates for aerocapture trajectories for β values of 1, 10, and 100 kg/m^2; radiative heating effects are not included. For a spacecraft mass of 1500 kg, these β values correspond to diameters of approximately 3.4, 10.6, and 33.5 m, respectively. The data in Fig. 10 represent bounding peak heat rates over potential aerocapture corridors. For example, aerocapture at Mars with an AI velocity of 6 km/s, a β_1 of 10 kg/m^2, and a β-ratio of 10 may experience peak convective peak heat rates between 10 and 30 W/cm^2. A 400 km transfer orbit apoapsis altitude target was used for Mars and Venus and 1700 km was used for Titan. While heat rate limits for insulating thermal protection systems (TPS) are material specific, typical limits are well below 100 W/cm^2 for current flexible insulating TPS for suitable for inflatable decelerator systems. Therefore, 100 W/cm^2 was adopted as a conservative upper bound on the capabilities of flexible insulating TPS. Higher heat rates require an ablative TPS, which may require a rigid heat shield. Therefore, the insulating TPS heat rate limit may be seen as a delimiter between currently available inflatable decelerators and traditional rigid aeroshells.

The peak heat rates in Fig. 10 indicate that aerocapture at Venus requires a low β to limit the peak heat rate if current inflatable decelerators are to be used. Additionally, at the high velocities associated with Venus aerocapture, the radiative contribution to total heat rate may be equal to or greater than the convective contribution, increasing the peak heat rate the TPS must accommodate. For Mars, the radiative component of heating is typically small or negligible,[24] indicating that inflatable decelerators may be used for aerocapture. Radiative heating may also be significant at Titan and may lead to a requirement for a low β or ablative TPS.[21]

These results allow one to draw preliminary conclusions on the feasibility of using drag-only flight control for aerocapture. For Mars missions, adequate flight-path corridor width to accommodate uncertainties is provided by current approach navigation precision and β-ratios of less than 10.[20] Additionally, low heat rates at Mars make the use of lightweight HIAD drag skirts possible. Together, these make Mars an attractive target for drag modulation aerocapture systems. At Venus, expected peak heat rates require large diameter drag skirts to lower β to limit peak heat rates such that current inflatable TPS technology may be used. Smaller drag skirts may be used, but will require ablative TPS. However, aerocapture at Venus still requires β-ratios near 10 to provide adequate corridor width, independent of the specific drag modulation system selected. The requirement for either a very large drag skirt using existing flexible TPS or ablative TPS for a moderately large drag skirt create a system that is likely not mass competitive with traditional lift modulation systems. This makes Venus an unattractive target for drag modulation aerocapture. Conclusions about drag modulation aerocapture at Titan are less clear: while large flight-path angle corridor widths are available for reasonable β-ratios, distance from Earth and limited flight experience make approach navigation

American Institute of Aeronautics and Astronautics

less precise at Titan than in the inner Solar System. Also, while convective heat rates are below the insulating TPS limit for AI velocities below 9 km/s, radiative heating is expected to contribute significantly to total heating at Titan.[21] Therefore, drag modulation aerocapture at Titan may be attractive if the AI velocity or β are sufficiently low for use of insulating flexible TPS, if flexible ablative TPS is developed, or if navigation precision is sufficient to allow a low β-ratio rigid drag skirt with an ablative TPS to be used.

For these reasons, the remainder of this study focuses on drag modulation flight control aerocapture missions to Mars and Titan.
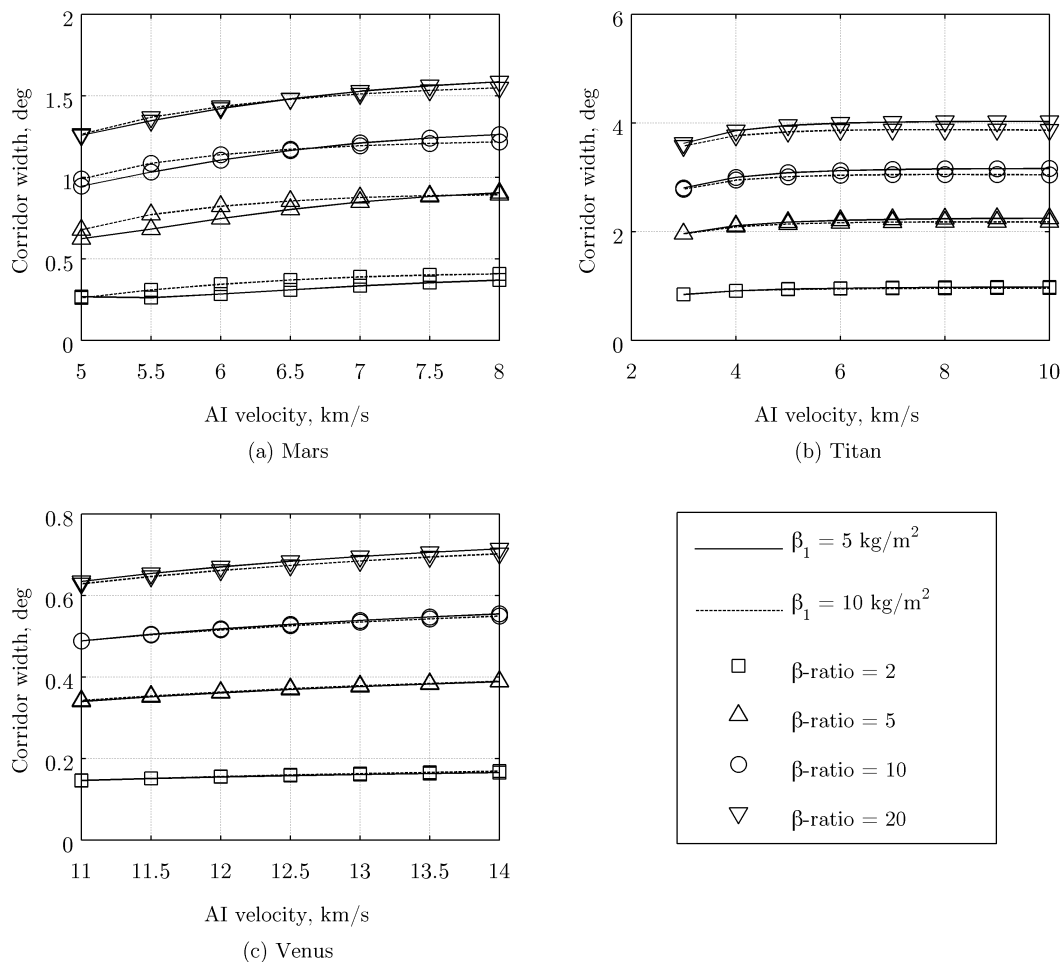
Figure 9. Aerocapture aerodynamic corridor widths at (a) Mars, (b) Titan, and (c) Venus for two values of β_1 and several β-ratios.

V. Aerocapture at Mars

A Mars science orbiter concept vehicle is used to evaluate three drag modulation system options for aerocapture. The spacecraft mass is nominally 1500 kg, corresponding to the Mars Reconnaissance Orbiter (MRO), less the propellant required for a Mars orbit insertion burn.[25] The spacecraft is packaged behind a 4 m diameter lightweight heat shield, producing a β_2 value of 70.2 kg/m^2. This diameter provides space for a MRO-sized 3 m diameter high-gain antenna. An eastbound equatorial trajectory is used, with a nominal AI inertial velocity of 6 km/s and a nominal AI inertial flight-path angle of -11.11 deg. The AI flight-path angle was selected to center the apoapsis altitude target within the vehicle's capability. The target orbit is a 400 km circular orbit.

American Institute of Aeronautics and Astronautics
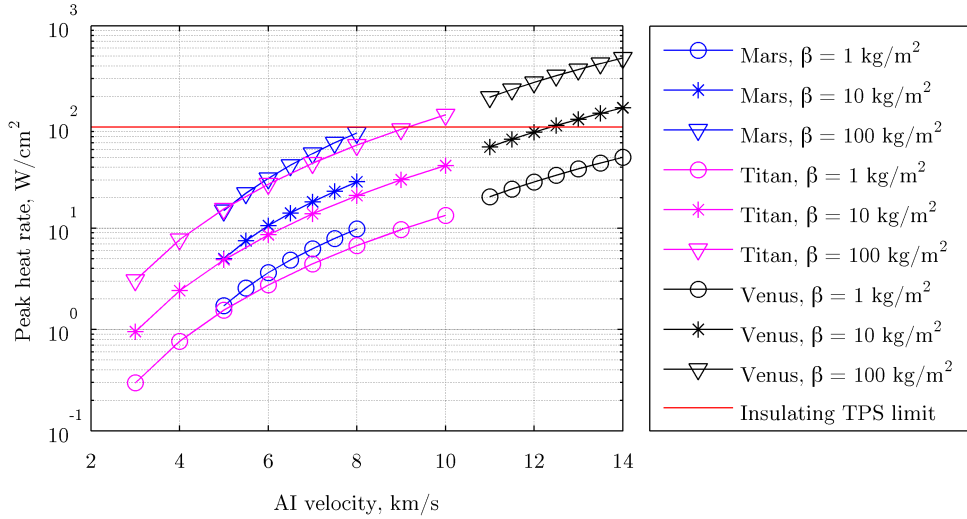
Figure 10. Peak stagnation-point convective heat rates for several β.

The single-stage system utilizes a HIAD drag skirt, which is deployed prior to AI to increase vehicle drag area. The inflation pressure is assumed to be sufficient to maintain a 70-deg spherecone shape throughout the atmospheric pass. The skirt has an outer diameter of 12.65 m, resulting in a β_1 of 7.02 kg/m^2 and a β-ratio of 10.

Results are provided in Fig. 11 and Table 3 for a 1000-sample Monte Carlo simulation. Sufficient apoapsis altitude accuracy is achieved to limit the mean+3σ total ΔV required to 110.7 m/s. Additionally, apoapsis error is roughly centered about the target, indicating good guidance algorithm performance. For all samples, peak deceleration is below 4 g and peak heat rates are below 15 W/cm^2, low enough to allow use of currently available insulating flexible TPS. Out-of-plane errors are minimal, with final transfer orbit inclinations near zero. Jettison times selected by the guidance algorithm range from about 160 s to 230 s (Fig. 11(a)). Maximum apoapsis errors are generally associated with the earliest jettison times: when the drag area must be jettisoned early in the trajectory, the vehicle is unable to account for dispersions encountered during the bulk of the atmospheric pass, leading to larger apoapsis altitude errors. As expected, Fig. 11(b) shows the magnitude of the periapsis raise ΔV does not vary significantly with apoapsis error, although lower energy cases with negative apoapsis errors require greater ΔV. The magnitude of the apoapsis correction ΔV is a strong function of apoapsis error, although most cases require less than 40 m/s of ΔV (Fig. 11(c)). While the accuracy of the single-stage system does not lead to large ΔV requirements, apoapsis error may be an issue for extreme cases, potentially causing reentry into the Mars atmosphere.

The two-stage jettison system was designed such that the first jettison event has a β-ratio of 5, while the second jettison even has a β-ratio of 2, resulting in a β_3 of 35.10 kg/m^2 and an inner skirt maximum diameter of 5.66 m; β_1 was retained from the single stage case. This split creates a course-fine control scheme, where the initial jettison event has more control authority to remove delivery error and predicted biases in aerodynamics and atmospheric properties and the second jettison event's lesser control authority is adequate to clean up any remaining error resulting from unforeseen biases or noise during the β_3 portion of the atmospheric pass.

Results for the two-stage system in Fig. 12 and Table 3. Using a second stage improves apoapsis accuracy and reduces the required propulsive ΔV, mostly through reducing the standard deviation of the apoapsis correction ΔV (Fig. 12(c)). Figure 12(a) shows the relationship between the first- and second-stage jettison times. The grey line denotes equal jettison times; the two circled cases jettison both stages at the same time to reduce their energy depletion rate early in the trajectory. Figures 12(b) and (c) also indicate a bias towards positive apoapsis error and the resulting retrograde apoapsis correction ΔV. Other performance metrics, including peak deceleration, peak heating, and heat load are similar to the single-stage system.

Results for a CV system with the same β_1 and β_2 (diameters of 12.65 and 4 m, respectively) as the staged-jettison cases are given in Fig. 13 and Table 3. Results indicate good aerocapture performance, with better apoapsis altitude accuracy, lower total ΔV requirements, and lower peak deceleration relative

American Institute of Aeronautics and Astronautics

to the staged-jettison systems. The accumulated out-of-plane error and aerothermal environments remain similar to the staged-jettison systems. Figure 13(a) shows that a significant amount of noise is present in the area command signal for some cases. However, for the nominal case, in black, the area command is nearly constant, validating the guidance algorithm's constant-area solution method.

The results presented indicate that single-stage, two-stage, and continuously-variable drag modulation systems are all feasible for aerocapture at Mars for the selected β-ratio of 10. However, a clear trend emerges in accuracy with the single-stage system being the least accurate and the CV system being the most accurate. The disparity in accuracy is highlighted in Fig. 14, which shows the high and low mean+3σ apoapsis errors. However, Fig. 14 also shows that, while better accuracy reduces the total ΔV required to circularize into a 400 km orbit, the difference in total ΔV between the three drag modulation system concepts is small. The CV system saves less than 15 m/s of ΔV which translates to a propellant mass savings of only about 10 kg for a 1500 kg spacecraft. However, the two-stage and CV systems provide additional robustness to uncertainty and design issues over the single-stage system, where atmospheric reentry may be more likely. Other trajectory metrics of interest are similar across all three systems, with the exception of peak deceleration, which is lower for the CV system.
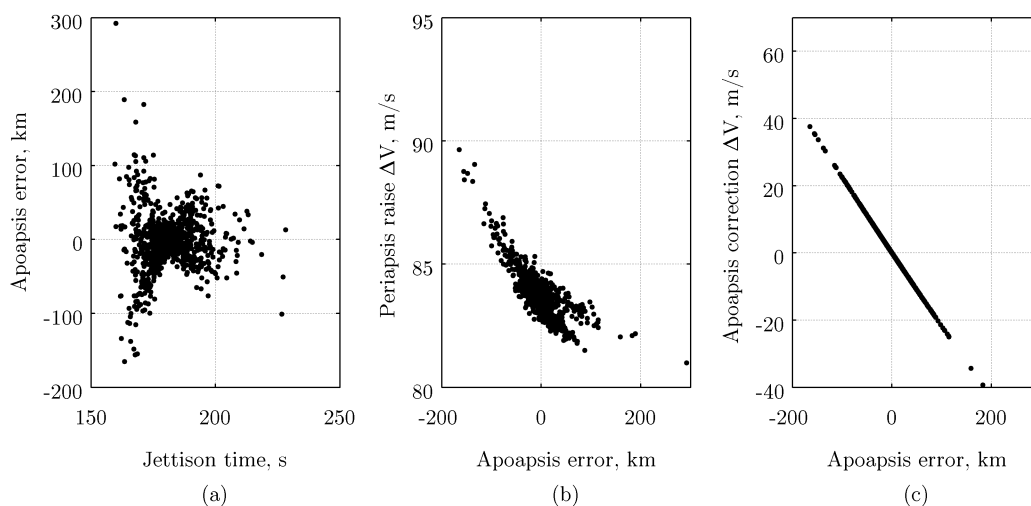
Figure 11. Monte Carlo results for single-stage system at Mars: (a) apoapsis error versus jettison time and (b) periapsis raise ΔV and (c) apoapsis correction ΔV versus apoapsis error.

VI. Aerocapture at Titan

The spacecraft concept used for Titan is based on the Titan Explorer Orbiter described in Ref. 18. The aerocapture vehicle has a nominal mass of 1800 kg. An eastbound equatorial trajectory is used, with a nominal AI inertial velocity of 6.5 km/s. The target orbit is a 1700 km circular orbit. The AI velocity and apoapsis target were selected to match the available literature.[8, 11, 18]

An initial single-stage system was designed to take advantage of the low β-ratio requirements at Titan. A 4.5 m rigid skirt was attached to a 3 m aeroshell, resulting in a β_1 of 66.6, a β_2 of 150 kg/m^2, and β-ratio of 2.25. This type of configuration may be assembled prior to launch and may use currently available ablative TPS to provide additional heat rate margin. The operational corridor for this vehicle was assessed by running 100-sample Monte Carlo simulations over a range of AI flight-path angles. A small sample size was chosen for this analysis to limit computation time. Results are presented in Fig. 15 and show that, while a β-ratio of 2.25 produces a nominal aerodynamic corridor width of about 1 deg (see Fig. 9), this configuration produces a zero-width operational corridor when uncertainties are included: there are no flight-path angles for which there are zero escape trajectories and zero reentry trajectories. This result was also found to be true for CV systems at this β-ratio, which exhibit the best possible drag modulation performance.

Therefore, a new drag modulation vehicle concept was formulated using a larger β-ratio. To reduce the severity of the aerothermal environment, a β_1 of 8 kg/m^2 was selected to limit the nominal convective
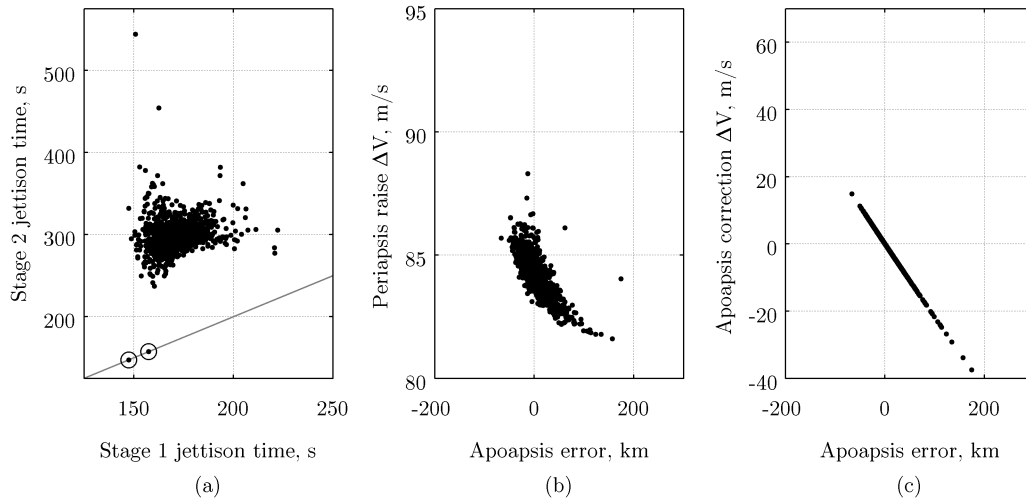
Figure 12. Monte Carlo results for two-stage system at Mars: (a) stage 2 versus stage 1 jettison time and (b) periapsis raise ΔV and (c) apoapsis correction ΔV versus apoapsis error.
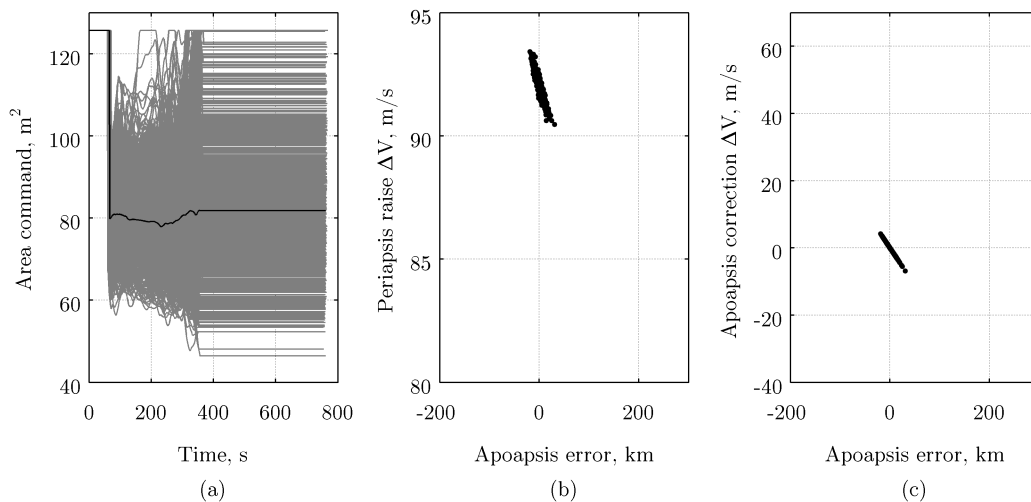

Figure 13. Monte Carlo results for CV system at Mars: (a) area command versus time (black curve denotes nominal) and (b) periapsis raise ΔV and (c) apoapsis correction ΔV versus apoapsis error.
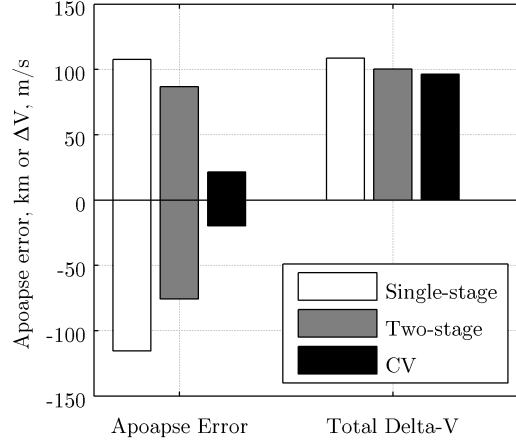
Figure 14. Comparison of drag modulation aerocapture system options for Mars.

Table 3. Monte Carlo Simulation Results for Drag Modulation Aerocapture at Mars

Parameter	Mean	σ	Mean-3σ	Mean$+3\sigma$	Min.	Max.
Single-stage system						
Apoapsis error, km	-3.923	37.197	-115.515	107.669	-164.918	292.231
Final inclination, deg	0.225	0.050	0.075	0.374	0.076	0.393
Periapsis raise ΔV, m/s	83.751	0.900	81.053	86.450	80.992	89.643
Apoapsis correction ΔV, m/s	0.921	8.233	-23.779	25.621	-61.839	37.601
Total ΔV, m/s	89.417	6.400	70.216	108.618	82.841	142.831
Peak deceleration, g	3.419	0.235	2.714	4.123	2.618	4.090
Peak conv. heat rate, W/cm^2	11.377	0.378	10.245	12.510	10.146	12.494
Integrated heat load, kJ/cm^2	1.819	0.100	1.519	2.120	1.415	2.089
Two-stage system						
Apoapsis error, km	5.567	27.109	-75.761	86.894	-66.423	173.939
Final inclination, deg	0.222	0.051	0.070	0.375	0.072	0.392
Periapsis raise ΔV, m/s	84.126	0.847	81.586	86.667	81.602	88.306
Apoapsis correction ΔV, m/s	-1.207	5.970	-19.116	16.702	-37.503	14.895
Total ΔV, m/s	88.604	3.886	76.946	100.262	83.698	121.538
Peak deceleration, g	3.419	0.235	2.714	4.123	2.618	4.090
Peak conv. heat rate, W/cm^2	11.377	0.378	10.245	12.510	10.146	12.494
Integrated heat load, kJ/cm^2	1.746	0.079	1.508	1.984	1.409	1.951
Continuously-variable system						
Apoapsis error, km	0.807	6.870	-19.804	21.418	-19.154	30.989
Final inclination, deg	0.177	0.048	0.034	0.321	0.042	0.336
Periapsis raise ΔV, m/s	92.015	0.470	90.606	93.425	90.465	93.426
Apoapsis correction ΔV, m/s	-0.177	1.523	-4.747	4.393	-6.838	4.262
Total ΔV, m/s	93.238	0.999	90.239	96.236	91.849	97.687
Peak deceleration, g	2.508	0.093	2.229	2.787	2.276	2.859
Peak conv. heat rate, W/cm^2	12.895	0.579	11.159	14.632	10.985	14.785
Integrated heat load, kJ/cm^2	1.586	0.066	1.386	1.785	1.348	1.775

stagnation point peak heating to 10 W/cm^2 to allow use of a HIAD drag skirt. The heat rate limit provides margin for radiative heating effects. A new inner diameter of 4.5 m was selected to mitigate packaging difficulty and allow use of a large, non-deployable antenna, such as the 3 m high gain antenna baseline for the Titan Explorer study.[18] This concept has an overall β-ratio of 8.34 and a maximum diameter of 12.98 m when the drag skirt is fully deployed. The operational corridor for the second concept was found to be approximately 0.5 deg wide (Fig. 16), twice that required for the assumed approach navigation accuracy. The nominal AI flight-path angle was chosen to be -32.95 deg, the center of the operational corridor.

Results for 1000-sample Monte Carlo simulations of aerocapture for the single-stage, two-stage, and CV drag modulation systems with a β-ratio of 8.34 are summarized in Table 4. Figure 17 shows results for the single-stage system. The range of apoapsis altitude errors is larger than at Mars, but similar trends are visible: early jettisons tend to have larger apoapsis errors, and the periapsis raise ΔV is only a weak function of apoapsis error. Results for the two-stage system (Fig. 18) also show similar trends to Mars, although at Titan no cases jettisoned both stages at the same time (identical jettison times are indicated by the grey line). Lastly, results for the CV system are given in Fig. 19. Even in the nominal case, the area commands tend to decrease over time. This is due to the strong eastward winds in the Titan-GRAM atmosphere model that are not modeled in the guidance predictor. Just as at Mars, there is a trend of increasing accuracy and decreasing ΔV requirements from single-stage to two-stage to CV systems. The results also indicate peak convective heat rates remain below 14 W/cm^2, validating the choice of β_1 and allowing use of a HIAD with flexible insulating TPS.

Figure 20 shows a relative comparison of accuracy and total ΔV requirements. The trends are slightly different than at Mars. Due to the relatively long atmospheric flight times at Titan, the addition of second stage provides a relatively greater benefit over the single-stage system when compared to Mars. The two-stage system provides the best total ΔV performance. This is somewhat counterintuitive, as the CV system has significantly better apoapsis accuracy, resulting in apoapsis correction ΔV values that are half of the two-stage system. However, the CV system tends to remove more energy during the atmospheric pass relative to the two-stage system, even though it achieves the desired apoapsis altitude. This energy must then be replaced by the spacecraft propulsion system in the periapsis raise maneuver.
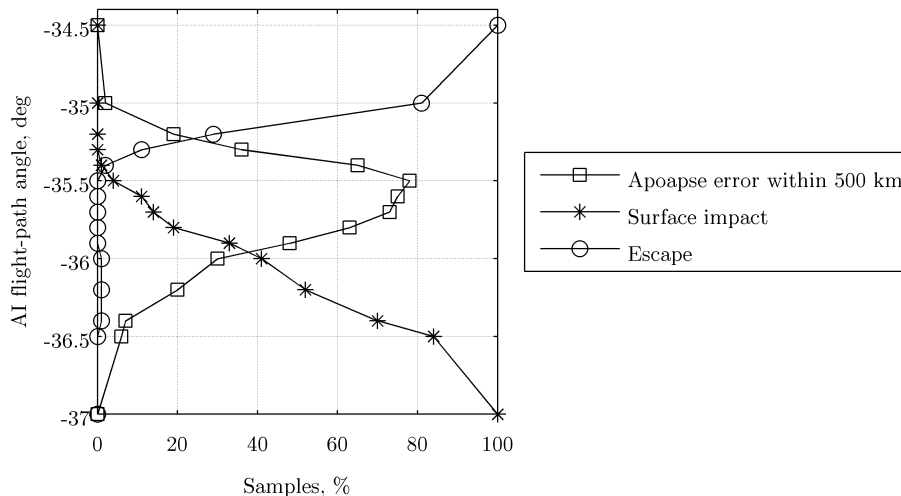

Figure 15. Operational corridor for single-stage aerocapture at Titan with a β-ratio of 2.25.

VII.   Discussion

Results indicate that drag modulation flight control presents an attractive option for aerocapture systems at Mars where low heat rates enable the use of large, lightweight, inflatable drag areas. The use of HIADs enables large β-ratios which provide a high degree of robustness to day-of-flight uncertainties, even for single-stage jettison systems. Drag modulation at Titan is found to require advanced non-ablative thermal protection systems for inflatable decelerators to withstand peak heat rates during the atmospheric pass or
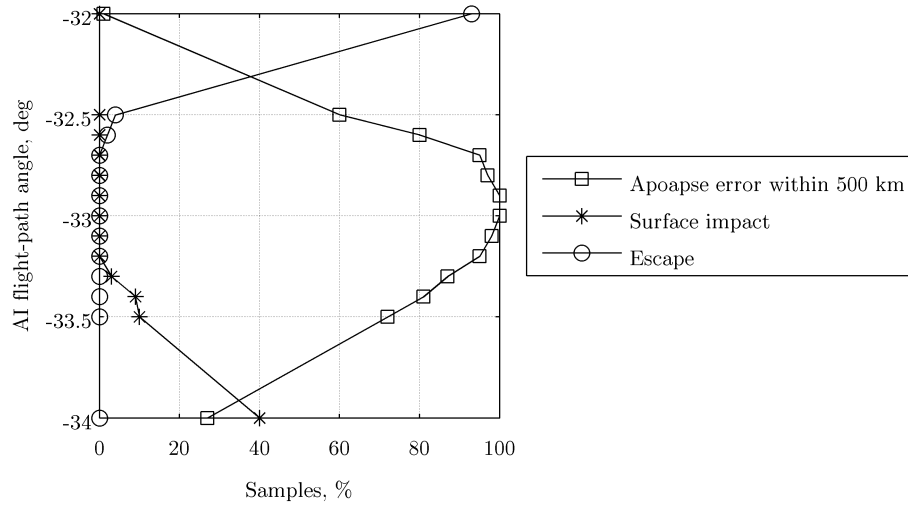
American Institute of Aeronautics and Astronautics

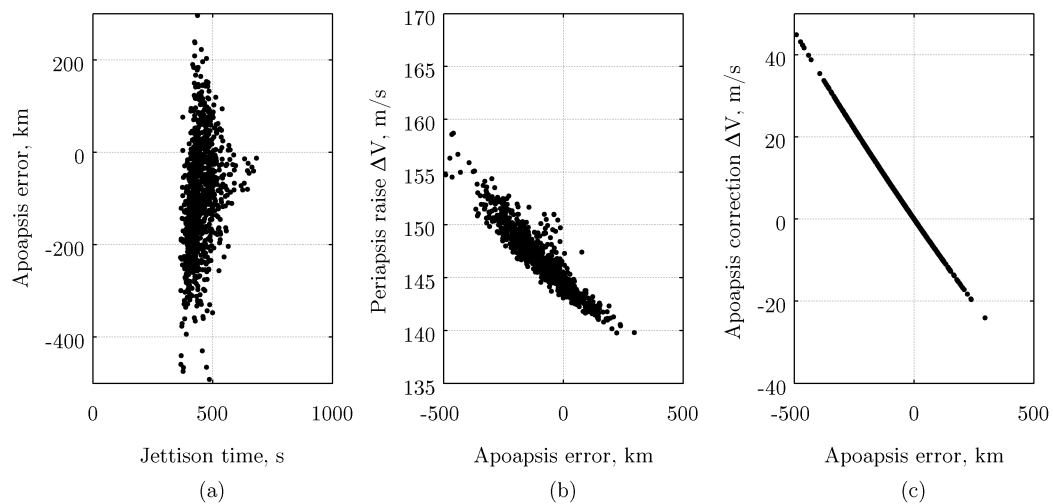**Figure 16. Operational corridor for single-stage aerocapture at Titan with a β-ratio of 8.34.**

Figure 17. Monte Carlo results for Titan single-stage system with β-ratio of 8.34: (a) apoapsis error versus jettison time and (b) periapsis raise ΔV and (c) apoapsis correction ΔV versus apoapsis error.
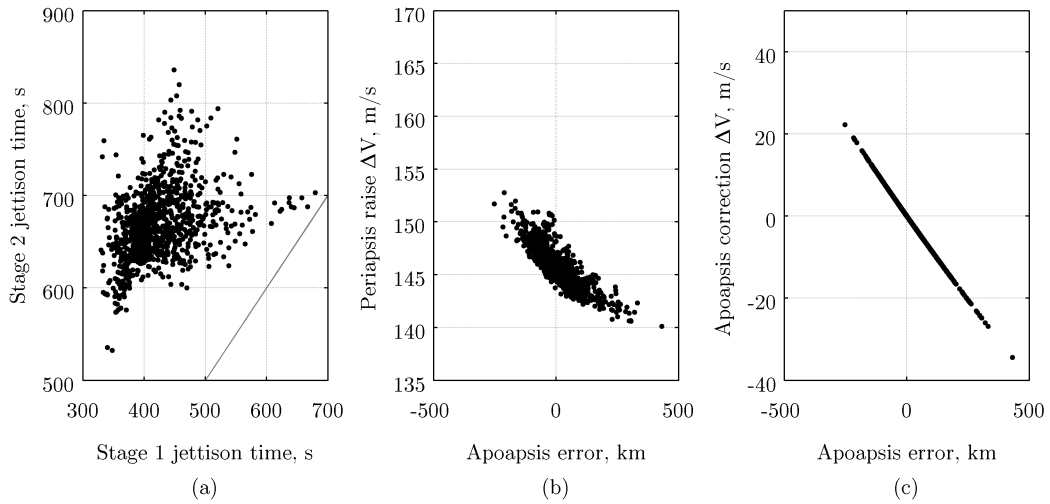
American Institute of Aeronautics and Astronautics

Figure 18. Monte Carlo results for Titan two-stage system with β-ratio of 8.34: (a) stage 2 versus stage 1 jettison time and (b) periapsis raise ΔV and (c) apoapsis correction ΔV versus apoapsis error.
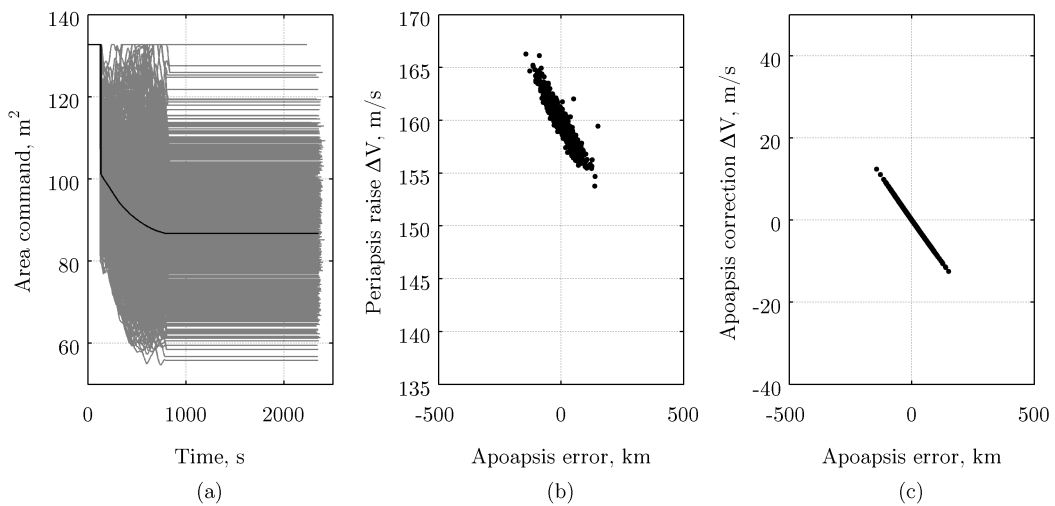

Figure 19. Monte Carlo results for Titan CV system with β-ratio of 8.34: (a) area command versus time (black curve denotes nominal) and (b) periapsis raise ΔV and (c) apoapsis correction ΔV versus apoapsis error.
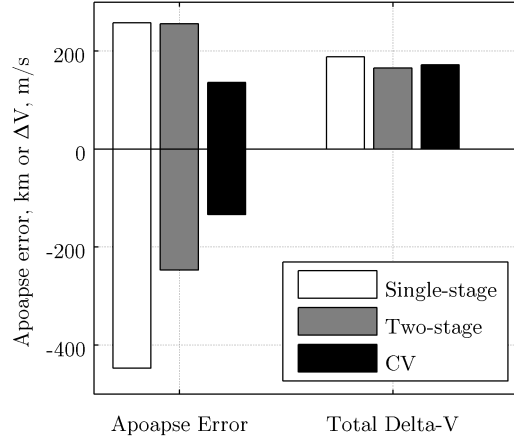
Figure 20. Comparison of drag modulation aerocapture system options for Titan.

Table 4. Monte Carlo Simulation Results for Drag Modulation Aerocapture at Titan with β-ratio of 8.34

Parameter	Mean	σ	Mean-3σ	Mean$+3\sigma$	Min.	Max.
Single-stage system						
Apoapsis error, km	-95.071	117.517	-447.624	257.481	-491.201	296.084
Final inclination, deg	0.644	0.478	-0.791	2.078	0.003	2.735
Periapsis raise ΔV, m/s	146.793	2.845	138.257	155.329	139.783	158.698
Apoapsis correction ΔV, m/s	8.350	10.265	-22.444	39.145	-24.055	44.864
Total ΔV, m/s	157.423	10.220	126.764	188.081	143.137	200.921
Peak deceleration, g	2.704	0.189	2.136	3.272	2.198	3.239
Peak conv. heat rate, W/cm^2	10.320	0.326	9.340	11.299	9.363	11.424
Integrated heat load, kJ/cm^2	2.034	0.051	1.882	2.186	1.900	2.187
Two-stage system						
Apoapsis error, km	4.351	83.777	-246.980	255.682	-252.540	431.480
Final inclination, deg	0.637	0.473	-0.781	2.054	0.004	2.742
Periapsis raise ΔV, m/s	145.743	1.913	140.006	151.481	140.120	152.775
Apoapsis correction ΔV, m/s	-0.283	7.023	-21.351	20.785	-34.405	22.226
Total ΔV, m/s	150.959	4.796	136.570	165.348	144.096	174.525
Peak deceleration, g	2.704	0.189	2.136	3.272	2.198	3.239
Peak conv. heat rate, W/cm^2	10.320	0.326	9.340	11.299	9.363	11.424
Integrated heat load, kJ/cm^2	2.030	0.050	1.880	2.180	1.900	2.188
Continuously-variable system						
Apoapsis error, km	1.056	44.916	-133.692	135.803	-143.653	150.247
Final inclination, deg	0.582	0.437	-0.730	1.894	0.008	2.682
Periapsis raise ΔV, m/s	159.870	1.918	154.115	165.625	153.785	166.277
Apoapsis correction ΔV, m/s	-0.065	3.805	-11.480	11.351	-12.461	12.437
Total ΔV, m/s	162.925	3.000	153.925	171.926	158.898	178.714
Peak deceleration, g	2.308	0.106	1.991	2.625	2.009	2.628
Peak conv. heat rate, W/cm^2	11.497	0.612	9.662	13.332	9.873	13.588
Integrated heat load, kJ/cm^2	2.258	0.111	1.925	2.592	1.942	2.581

American Institute of Aeronautics and Astronautics

large drag areas to limit peak heat rates to current non-ablative thermal protection system limits. Results indicate that a two-stage system with inflatable drag skirts provides acceptable orbital insertion performance with a potentially lower system complexity than comparable lift modulation systems. The large gravity well and high heat rates experienced during aerocapture at Venus make drag modulation flight control unattractive when combined with a non-ablative thermal protection system. Significantly larger drag areas or advances in fabric-based material thermal properties are required to improve feasibility at Venus.

Overall, drag modulation flight control is largely enabled by three technologies: precise approach navigation, modern flight computers, and HIADs. Current deep space navigation precision results in minimal delivery and knowledge errors at AI, making out-of-plane control optional in the absence of plane change requirements. Modern flight computers provide enough throughput to allow the use of onboard parameter estimation techniques coupled with numeric predictor-corrector algorithms, resulting in accurate terminal state predictions and steering commands. HIADs provide a mass efficient solution to lower the ballistic coefficient and achieve the required ballistic coefficient ratio and control authority.

Future work for drag modulation flight control aerocapture systems may include more detailed vehicle sizing, the development of more computationally efficient onboard guidance algorithms, and six-degree-of-freedom simulation. Six-degree-of-freedom simulation will allow study of vehicle stability across jettison events, separation dynamics, and recontact. Lastly, better engineering level models for radiative heating rates at Titan and Venus will help to reduce uncertainty and required TPS margin on future aerocapture vehicles.

Acknowledgement

References

[1]Cianciolo, A. M. D., Davis, J. L., Komar, D. R., Munk, M. M., Samareh, J. A., Powell, R. W., Shidner, J. D., Stanley, D. O., Wilhite, A. W., Kinney, D., McGuire, M. K., Arnold, J. O., Howard, A. R., Sostaric, R. R., Studak, J., Zumwalt, C. H., Llama, E. G., Casoliva, J., Ivanov, M. C., Clark, I. G., and Sengupta, A., "Entry, Descent and Landing Systems Analysis Study," Tech. Rep. NASA TM-2010-216720, July 2010.

[2]Cianciolo, A. M. D., Davis, J. L., Engelund, W. C., Komar, D. R., Queen, E. M., Samareh, J. A., Way, D. W., Zang, T. A., Murch, J. G., Krizan, S. A., Olds, A. D., Powell, R. W., Shidner, J. D., Kinney, D., McGuire, M. K., Arnold, J. O., Covington, M. A., Sostaric, R. R., Zumwalt, C. H., and Llama, E. G., "Entry, Descent and Landing Systems Analysis Study," Tech. Rep. NASA TM-2011-217055, Feb. 2011.

[3]Steinfeldt, B. A., Grant, M. J., Matz, D. A., Braun, R. D., and Barton, G. H., "Guidance, Navigation, and Control System Performance Trades for Mars Pinpoint Landing," *Journal of Spacecraft and Rockets*, Vol. 47, No. 1, Jan. 2010, pp. 188–198.

[4]Levy, L. L., "The Use of Drag Modulation to Limit the Rate at Which Deceleration Increases During Nonlifting Entry," Tech. Rep. NASA TN D-1037, Ames Research Center, Washington, DC, Sept. 1961.

[5]Rose, P. H. and Hayes, J. E., "Drag Modulation and Celestial Mechanics," *7th Annual Meeting of of the American Astronautical Society*, Dallas, TX, Jan. 1961.

[6]Kuo, Z.-S., Liu, K.-C., and Chang, Y.-S., "Explicit Guidance of Ballistic Entry Using Improved Matched Asymptotic Expansions," *Transactions of the Japan Society for Aeronautical and Space Sciences*, Vol. 50, No. 168, Jan. 2007, pp. 121–127.

[7]McRonald, A. D., "A Lightweight Inflatable Hypersonic Drag Device for Planetary Entry," *Association Aeronautique de France Conference*, Arcachon, France, March 1999.

[8]Westhelle, C. H. and Masciarelli, J. P., "Assessment of Aerocapture Flight at Titan Using a Drag-only Device," *AIAA Atmospheric Flight Mechanics Conference and Exhibit*, Austin, TX, Aug. 2003, pp. 1–7.

[9]Hall, J. L. and Le, A. K., "Aerocapture Trajectories for Spacecraft with Large Towed Ballutes," *AAS/AIAA Space Flight Mechanics Meeting*, Santa Barbara, CA, Feb. 2001.

[10]Miller, K. L., Gulick, D., Lewis, J., Trochman, B., Stein, J., Lyons, D. T., and Wilmoth, R. G., "Trailing Ballute Aerocapture: Concept and Feasibility Assessment," *39th AIAA/ASME/SAE/ASEE Joint Propulsion Conference and Exhibit*, Huntsville, AL, July 2003.

[11]Johnson, W. R. and Lyons, D. T., "Titan Ballute Aerocapture Using a Perturbed TitanGRAM Model," *AIAA Atmospheric Flight Mechanics Conference and Exhibit*, Providence, RI, Aug. 2004.

[12]Putnam, Z. R., Clark, I. G., and Braun, R. D., "Drag modulation flight control for aerocapture," *Aerospace Conference, 2012 IEEE*, 2012, pp. 1–10.

[13]Venkatapathy, E., Arnold, J., Fernandez, I., Hamm, K. R., Kinney, D., Laub, B., Makino, A., McGuire, M. K., Peterson, K., Prabhu, D., Empey, D., Dupzyk, I., Huynh, L., Hajela, P., Gage, P., Howard, A. R., and Andrews, D., "Adaptive Deployable Entry and Placement Technology (ADEPT): A Feasibility Study for Human Missions to Mars," *21st AIAA Aerodynamic Decelerator Systems Technology Conference and Seminar*, Dublin, Ireland, May 2011.

[14]Duvall, A. L., Justus, C. G., and Keller, V. W., "Global Reference Atmospheric Model (GRAM) Series for Aeroassist Applications," *43rd AIAA Aerospace Sciences Meeting and Exhibit*, Reno, NV, Jan. 2005.

[15]Sutton, K. and Graves, R. A., "A General Stagnation-point Convective-heating Equation for Arbitrary Gas Mixtures," Tech. Rep. NASA TR R-376, NASA, Washington, DC, Nov. 1971.

[16]Kinney, D., "Aero-Thermodynamics for Conceptual Design," *42nd AIAA Aerospace Sciences Meeting and Exhibit*, Reno, Nevada, Jan. 2004, pp. 1–11.

[17]Martin-Mur, T. J., Kruizinga, G. L., and Wong, M. C., "Mars Science Laboratory Interplanetary Navigation Analysis," *21st International Symposium in Space Flight Dynamics*, San Jose dos Campos, Brazil, Jan. 2011, pp. 1–15.

[18]Lockwood, M. K., Leary, J. C., Lorenz, R., Waite, H., Reh, K., Prince, J., and Powell, R. W., "Titan Explorer," *AIAA/AAS Astrodynamics Specialist Conference and Exhibit*, Honolulu, HI, Aug. 2008.

[19]Hanak, C. and Bishop, R. H., "Aerocapture at Titan and Neptune: Navigation Sensitivity Study," *9th AIAA Atmospheric Flight Mechanics Conference*, University of Texas, Providence, RI, Aug. 2004.

[20]Striepe, S. A., Way, D. W., and Dwyer, A. M., "Mars Science Laboratory Simulations for Entry, Descent, and Landing," *Journal of Spacecraft and Rockets*, Vol. 43, No. 2, March 2006, pp. 311–323.

[21]Lockwood, M. K., "Titan Aerocapture Systems Analysis," *39th AIAA/ASME/SAE/ASEE Joint Propulsion Conference and Exhibit*, Huntsville, AL, July 2003.

[22]Wooster, P. D., Braun, R. D., Ahn, J., and Putnam, Z. R., "Mission design options for human Mars missions," *MARS*, 2007.

[23]Craig, S. and Lyne, J. E., "Parametric Study of Aerocapture for Missions to Venus," *Journal of Spacecraft and Rockets*, Vol. 42, No. 6, Nov. 2005, pp. 1035–1038.

[24]Tauber, M. E. and Sutton, K., "Stagnation-point Radiative Heating Relations for Earth and Mars Entries," *Journal of Spacecraft and Rockets*, Vol. 28, No. 1, June 2003, pp. 40–42.

[25]Graf, J. E., Johnston, M. D., Zurek, R. W., De Paula, R. P., Eisen, H. J., and Jai, B., "The Mars Reconnaissance Orbiter Mission," *54th International Astronautical Congress*, Bremen, Germany, Oct. 2003.